Utilization of a nitrogen–sulfur nonbonding interaction in the design of new 2-aminothiazol-5-yl-pyrimidines as p38α MAP kinase inhibitors

Shuqun Lin [a], Stephen T. Wrobleski [a,*], John Hynes Jr. [a], Sidney Pitt [b], Rosemary Zhang [b], Yi Fan [b], Arthur M. Doweyko [c], Kevin F. Kish [c], John S. Sack [c], Mary F. Malley [c], Susan E. Kiefer [c], John A. Newitt [c], Murray McKinnon [b], James Trzaskos [b], Joel C. Barrish [a], John H. Dodd [a], Gary L. Schieven [b], Katerina Leftheris [a]

[a] Department of Immunology Chemistry, Bristol-Myers Squibb Pharmaceutical Research Institute, Princeton, NJ 08543-4000, USA
[b] Department of Immunology Biology, Bristol-Myers Squibb Pharmaceutical Research Institute, Princeton, NJ 08543-4000, USA
[c] Department of Molecular Biosciences, Bristol-Myers Squibb Pharmaceutical Research Institute, Princeton, NJ 08543-4000, USA

ARTICLE INFO

ABSTRACT

The design, synthesis, and structure–activity relationships (SAR) of a series of 2-aminothiazol-5-yl-pyrimidines as novel p38α MAP kinase inhibitors are described. These efforts led to the identification of **41** as a potent p38α inhibitor that utilizes a unique nitrogen–sulfur intramolecular nonbonding interaction to stabilize the conformation required for binding to the p38α active site. X-ray crystallographic studies that confirm the proposed binding mode of this class of inhibitors in p38α and provide evidence for the proposed intramolecular nitrogen–sulfur interaction are discussed.

© 2010 Elsevier Ltd. All rights reserved.

Inhibiting the p38 MAP kinase pathway in vivo is known to be effective in controlling the release of various proinflammatory cytokines, most notably TNF-α and IL-1β.[1] As a result, small molecule p38 inhibitors have attracted interest within the pharmaceutical industry due to the potential to effectively treat significant inflammatory diseases such as rheumatoid arthritis.[2] We have previously reported the discovery of several novel classes of p38 inhibitors which include potent 2-aminothiazoles such as **1**.[3] Based on the known binding interactions of **1** in the p38α active site, we have recently developed 2-aminothiazol-5-yl-pyrimidines having the general structure **2** as novel p38α inhibitors (Fig. 1). Herein, we wish to report the design, synthesis, and SAR of this new class of inhibitors which utilize a unique intramolecular nitrogen–sulfur nonbonding interaction to stabilize the preferred conformation for binding to p38α. X-ray crystallographic studies that confirm the p38α binding mode and provide evidence for the proposed non-bonding interaction are discussed herein.

The primary objective of these efforts was to design structurally diverse classes of p38 inhibitors for evaluation as potential drug candidates. Since other in-house developed p38 inhibitors including **1** utilized the 3-amino-4-methylbenzamide pharmacophore, the proposed 2-aminothiazol-5-yl-pyrimidines (**2**) represented a

structurally unique series for investigation. Molecular modeling analysis using structures derived from **2** revealed the potential ability of the pyrimidine phenyl substituent to probe deeper into the lipophilic pocket (P1), normally referred to as the kinase selectivity pocket, relative to **1** while still maintaining key hydrogen bond interactions between the nitrogen atom on the thiazole moiety and the p38 Met109 residue as in **1** (Fig. 2). In addition, the new design incorporated a pyrimidine ring to favor the proposed bioactive conformation whereby one of the pyrimidine nitrogens could
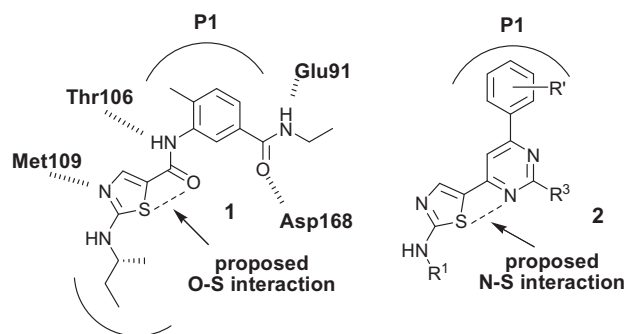
Figure 1. Key interactions of **1** with p38α based on X-ray and proposed binding mode of novel 2-aminothiazol-5-yl-pyrimidines **2**.

* Corresponding author. Tel.: +1 609 252 4873; fax: +1 609 252 7410.
E-mail address: stephen.wrobleski@bms.com (S.T. Wrobleski).
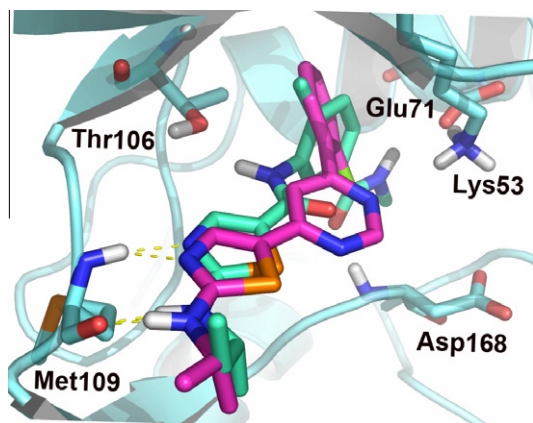
Figure 2. X-ray structure of p38α complex with **1** (in turquoise) in the ATP site with an overlay based on molecular modeling of a proposed thiazole-pyrimidine analog **2** (in magenta where R^1 = *i*-Pr, R^3 = hydrogen and R′ = chloro).

engage in a stabilizing intramolecular $n_o \rightarrow \sigma^*$ nonbonding interaction with the thiazole sulfur atom. Related types of sulfur–heteroatom interactions have been previously reported[4a–c] and were believed to be important in analogs such as **1** where the amide carbonyl oxygen and the thiazole sulfur atom formed a similar stabilizing interaction to favor potent binding to p38α.

Synthesis of the targeted pyrimidines **2** were initially undertaken as outlined in Scheme 1. This route utilized condensation of thiourea **3** with DMF–DMA to yield **4** followed by thiazole ring formation by base-mediated cyclization with chloroacetone to afford ketone **5**. Formation of the pyrimidine ring was accomplished by condensation with benzaldehydes to give enone **6** and cyclization with available amidines or guanidines to yield the targeted analogs **2**. An improved synthesis to incorporate amino groups at the pyrimidine 2-position is outlined in Scheme 2. This route utilized a novel 2-aminothiazole-5-boronate ester **9** as a key intermediate which enabled a highly modular and efficient synthesis from commercially available reagents. This key intermediate was readily prepared from commercially available 2-amino-5-bromothiazole (**7**) via Boc protection and subsequent coupling with alcohols under Mitsunobu conditions to install the R^1 substituent affording **8**. Lithium–halogen exchange followed by borylation in high yields[5] afforded the key thiazole boronate ester **9** as a bench stable solid. Efficient cross-coupling of **9** with commercially available 2-thiomethyl-4,6-dichloro-pyrimidine under standard Suzuki–Miyaura coupling conditions afforded **11**. Finally, sequential cleavage of the Boc protecting group, oxidation to the sulfone, and displacement with amines at the C-2 position of the pyrimidine ring
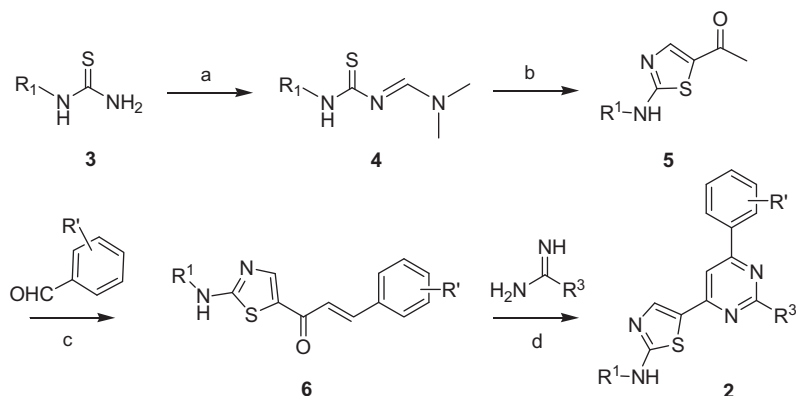
Scheme 1. Reagents and conditions: (a) DMF–DMA, EtOH, 90 °C, 90–95%; (b) chloroacetone, CH$_3$CN, 65 °C, then TEA, 72–97%; (c) aq KOH, EtOH, 90 °C, 35–80%; (d) NaOEt, EtOH, 20–63%.
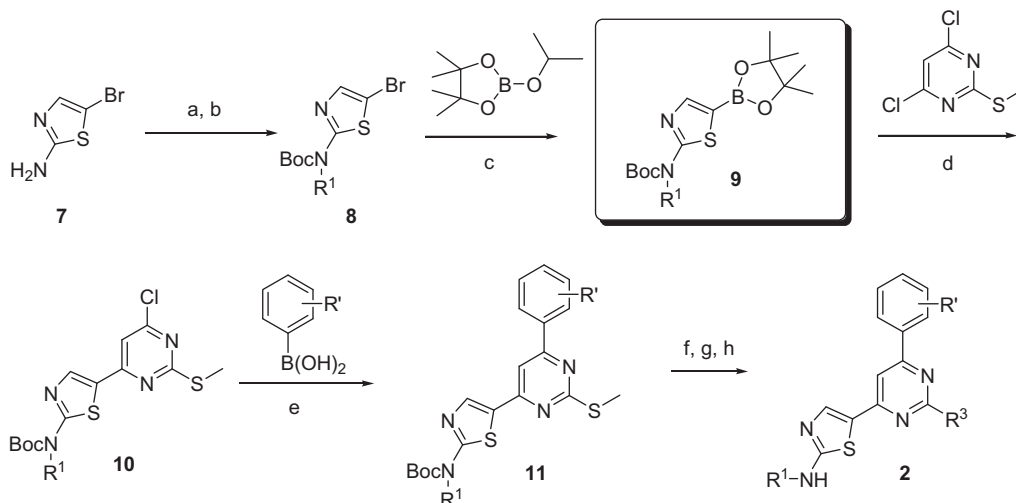
Scheme 2. Reagents and conditions: (a) Boc$_2$O, pyridine, quant.; (b) R^{1}OH, PPh$_3$, DEAD, THF, 76–80%; (c) *n*-BuLi, THF; (d) Pd(PPh$_3$)$_4$, K$_3$PO$_4$, EtOH, toluene, >95%; (e) Pd(PPh$_3$)$_4$, K$_3$PO$_4$, EtOH, toluene, 63–78%; (f) TFA, quant.; (g) oxone, aq MeOH, 80–95%; (h) amines, *i*-PrOH, 120 °C, 43–55%.
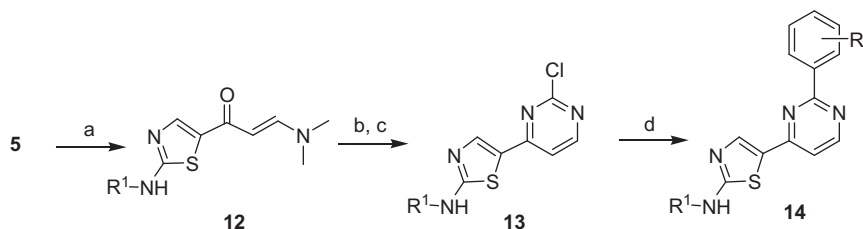
Scheme 3. Reagents and conditions: (a) DMF–DMA, 100 °C, 65–73%; (b) NaH, urea, 57–70%; (c) POCl₃, toluene, 110 °C, 60–80%; (d) aryl boronic acid, Pd(PPh₃)₄, 2 M aq K₃PO₄, EtOH, toluene (19–29%).

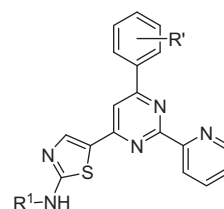afforded the targeted compounds **2**. For SAR comparison, the isomeric pyrimidines were also prepared as in Scheme 3. Condensation of ketone **5** with DMF–DMA yielded the vinylogous amide **12** followed by condensation with urea and chlorination to provide **13**. Suzuki–Miyaura coupling then afforded the isomeric thiazole-pyrimidines **14**.

Final compounds were tested in an assay that measured inhibition of human p38α enzyme activity.[6] Initial investigations explored R^2 and R^3 pyrimidine ring substitutions as shown in Table 1. An ortho substituted phenyl group (2-fluorophenyl) was incorporated at R^2 (**15–17**) since molecular modeling docking studies suggested a small ortho substituent may be favorable to orient the phenyl ring out of plane with respect to the pyrimidine ring (vide infra). Initial groups that were explored at R^3 showed a preference for an amino substitution as opposed to small alkyl groups (compare **15** vs **16** and **17**). To explore an alternative pyrimidine isomer, the 2-fluorophenyl group was also incorporated at the R^3 position with R^2 = H as in **18**. However, isomer **18** was found to be inactive at concentrations below 30 μM. Replacement of the 2-fluorophenyl group at R^3 in **18** with alkyl groups (**19**) resulted in a loss in activity whereas a 2-pyridyl group (**20**) was found to have notable activity (IC$_{50}$ = 314 nM). On the basis of these observations, the 2-fluorophenyl group was incorporated at R^2 while maintaining the more optimal 2-pyridyl at R^3 to afford **21** which gave ca. 5-fold improvement in potency (IC$_{50}$ = 52 nM) compared to **15** (IC$_{50}$ = 225 nM). This analog represented the most potent compound from these initial SAR explorations and subsequent efforts sought to optimize the potency around this series.

Optimization of both the phenyl group substitution (R′) and aminothiazole group (R^1) was explored next (Table 2). Potent analogs were evaluated in a cell-based functional assay that measured the inhibition of TNF-α biosynthesis in human peripheral blood
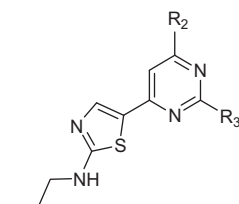
Table 1
Initial pyrimidine SAR at R^2 and R^3 positions

Compd	R^2	R^3	p38α IC$_{50}$, nM
15	2-F-phenyl	–NH₂	225
16	2-F-phenyl	–CH₃	520
17	2-F-phenyl	cyc-Pr	>1000
18	H	2-F-phenyl	>30,000
19	H	cyc-Pr	>1000
20	H	2-Pyridyl	314
21	2-F-phenyl	2-Pyridyl	52

Table 2
SAR of 2-pyridyl analogs

Compd	R^1	R′	p38α IC$_{50}$, nM	PBMC IC$_{50}$, nM
22	n-Pr	2-F	52	62
23	n-Pr	2-Cl	22	17
24	n-Pr	2-OEt	859	—
25	n-Pr	2-Cl, 4-F	42	17
26	n-Pr	2-Cl, 4-OEt	3940	—
27	H	2-Cl	114	—
28	Et	2-Cl	17	119
29	cyc-Pr	2-Cl	17	22
30	cyc-Bu	2-Cl	16	28
31	iso-Pr	2-Cl	4	21
32	(S)-sec-Bu	2-Cl	8	31
33	(R)-sec-Bu	2-Cl	5	13

mononuclear cells (PBMCs).[7] With n-Pr at R^1, replacement of the 2-fluorophenyl (**22**) with 2-chlorophenyl (**23**) resulted in an ca. 2-fold increase in enzyme potency and ca. 3–4-fold improvement in cellular potency (Table 2). Incorporation of larger ortho groups such as ethoxy (**24**) was not well tolerated. Substitution at the para position of the phenyl group was also explored, however, only small groups such as fluoro (**25**) were tolerated. Using the optimal 2-chlorophenyl group, optimization of the aminothiazole R^1 substituent was then investigated (**27–33**). Small branched alkyl groups proved to be optimal for potency, a finding that is consistent with the aminothiazole group binding to the p38 hinge region as previously reported for **1**.[3a] The isopropyl analog **31** and the (R)-sec-butyl analog **33** were most potent against the enzyme and were also among the most potent analogs in the cellular assay.
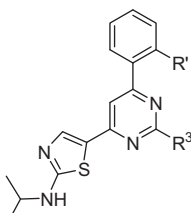
Despite achieving promising potency with compounds **31–33**, these analogs suffered from poor physicochemical properties such as low aqueous solubility (amorphous solubility <0.005 mg/mL at pH 6.5) and high clog P values >5. In addition, modest selectivity versus other kinases such as LIMK1 and LIMK2 were also observed for analogs from this series (LIMK1 and LIMK2 IC$_{50}$'s = 252 and 362 nM, respectively, for **31**). To further improve the kinase selectivity profile within the series, additional R′ phenyl substituents were explored given the groups proposed residence within the p38 kinase selectivity pocket (P1). Furthermore, polar non-aromatic groups were incorporated at the R^3 position to improve physicochemical properties. In analogy to earlier SAR (e.g., **15**, Table 1), optimization commenced with installation of polar amino substituents at R^3 (**34–39**, Table 3). Tertiary amino groups were

Table 3
SAR of phenyl R^2 group and pyrimidine R^3 group

Compd	R′	R^3	p38α IC$_{50}$, nM	PBMC IC$_{50}$, nM
34	–Cl	–H	46	31
35	–Cl	–NH$_2$	16	>250
36	–Cl	–N(CH$_3$)$_2$	573	—
37	–Cl	–NCH$_2$CH$_2$N(CH$_3$)$_2$	5	1
38	–Cl	–NHCH$_2$CH$_2$OH	8	8
39	–Cl	NHCH$_2$CH(OH)CH$_2$OH	6	11
40	(methyl urea)	–NCH$_2$CH$_2$N(CH$_3$)$_2$	2	12
41	(ethyl urea)	–NCH$_2$CH$_2$N(CH$_3$)$_2$	7	3
42	(cyclopropyl urea)	–NCH$_2$CH$_2$N(CH$_3$)$_2$	16	11

Figure 3. Binding interactions between **41** and unphosphorylated p38α based on X-ray crystallographic analysis. Hydrogen bond distances are based on hydrogen to heavy atom distances and are given in angstroms with key protein residues labeled. Protein carbons are drawn in turquoise and inhibitor carbons in white. PDB code 3NWW.

generally not well tolerated at R^3 (**36**) while secondary amino groups were most favored. Analogs containing an additional polar amine or alcohol functionality (**37**–**39**) were most potent achieving single-digit nanomolar potency in both the enzyme and cellular assays (**37** and **38**). Furthermore, **37** was found to have significantly improved aqueous solubility (0.994 mg/mL at pH 6.5) and decreased potency versus LIMK1 and LIMK2 (IC$_{50}$'s = 4.01 and 3.05 μM, respectively) relative to the 2-pyridyl analog **31**.

To improve kinase selectivity, incorporation of R′ groups capable of additional hydrogen bond interactions within the p38 active site were investigated. Molecular modeling studies suggested a pendant urea functionality at R′ may be able to engage the Glu71 and Asp168 residues as previously reported for **1**.[3a] To this end, the methyl, ethyl and cyclopropyl ureas (**40**–**42**) were prepared. Gratifyingly, the ethyl urea **41** showed a similar level of potency versus the enzyme and in cells relative to the 2-chlorophenyl analog **37**. Moreover, **41** gave improved aqueous solubility using amorphous material (5.94 mg/mL at pH 6.5), >10,000-fold selectivity versus LIMK1 and LIMK2 and a good overall kinase selectivity profile with the most cross-reactivity being observed for JNK3.[8]

To confirm the proposed binding mode of this class of p38 inhibitors, an X-ray crystallographic structure of **41** bound in the active site of unphosphorylated p38α enzyme was obtained (Fig. 3). As similarly reported for **1**,[3a] the 2-aminothiazole group of **41** forms dual hydrogen bonds (1.80 and 2.11 Å as measured by hydrogen to heavy atom distances) with the p38 hinge region Met109 residue. In addition, the phenyl group projects deep into the lipophilic selectivity pocket (P1) and lies nearly orthogonal relative to the pyrimidine core as originally proposed by molecular modeling studies. This finding also explains the preference for ortho substituents on the phenyl ring which favors nonplanarity. Furthermore, the pendant urea forms key hydrogen bond interactions with the active site Glu71 and Asp168 as was originally designed. More specifically, both urea hydrogens participate in a bidentate hydrogen bond interaction with Glu71 (2.18 and
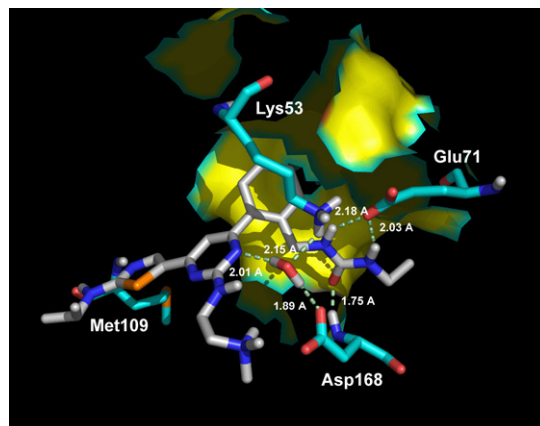
2.03 Å) with the urea carbonyl also forming a hydrogen bond to the Asp168 backbone N–H (1.75 Å). The structure also reveals a water molecule forming a hydrogen bond network between the pyrimidine nitrogen and the conserved Asp168 and Lys53 side chains. The previously noted preference for polar substituents at the pyrimidine 2-position can be explained by noting that this group projects into the polar ATP ribose binding region near the Asp168 residue within the active site.

Also noteworthy from the X-ray structure of **41** is the coplanarity of the thiazole and pyrimidine rings having the thiazole sulfur atom positioned in close proximity to one of the pyrimidine nitrogens. This result supports the proposed intramolecular $n_o \rightarrow \sigma^*$ nonbonding interaction between the nitrogen and sulfur atoms in stabilizing the bioactive conformation as previously discussed. To provide additional evidence for this hypothesis, small molecule X-ray crystal structures were obtained for the pyrimidine isomers **34** and **43** (Fig. 4). As anticipated, the more potent analog **34** having the same pyrimidine isomer as in **41** crystallized in the bioactive conformation. Close analysis of this structure revealed a short nitrogen-to-sulfur contact distance of 2.90 Å which is significantly

34
p38 IC$_{50}$ = 46 nM

43
p38 IC$_{50}$ = 223 nM
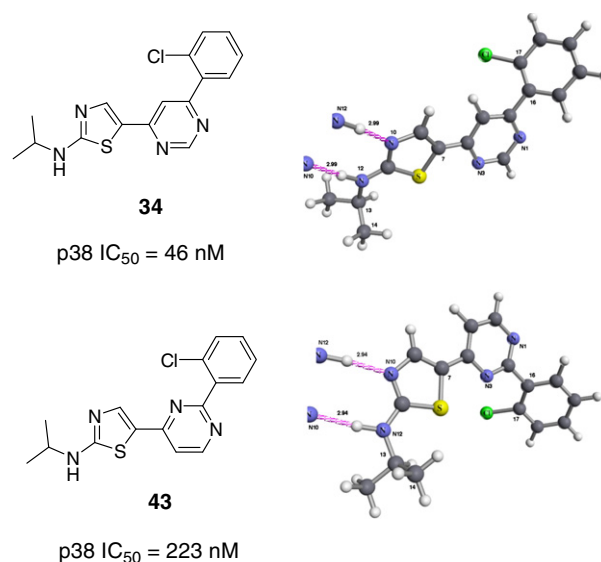
Figure 4. Single crystal X-ray crystallographic structures of isomers **34** and **43**. CCDC codes 783565 and 783566, respectively.

shorter than the sum of the van der Waals radii of nitrogen and sulfur atoms (3.35 Å) indicative of a stabilizing nonbonding interaction. Furthermore, the less potent pyrimidine isomer **43** also crystallized in a conformation having a short nitrogen-to-sulfur contact distance of 2.94 Å indicating a similar nonbonding interaction. However, in the case of **43**, this conformation is not the preferred conformation for binding to p38, and as such, provides an explanation for the decreased potency observed for this isomer.

In conclusion, we have designed and synthesized 2-aminothiazol-5-yl-pyrimidines as a novel series of potent and selective p38α inhibitors. These SAR efforts were performed with the aim of identifying structurally unique p38α inhibitors having a suitable balance of potency and physicochemical properties and were guided by structure-based design principles leading to the discovery of **41** as a promising analog for further investigation. Highlights of these efforts also include the use of a novel 2-aminothiazole-5-boronate ester intermediate to enable a highly modular synthesis of the targeted compounds and the use of a unique intramolecular nitrogen–sulfur nonbonding interaction to stabilize the conformation required for binding to p38α as supported by X-ray crystallographic data.

Acknowledgement

References and notes

1. (a) Adams, J. L.; Badger, A. M.; Kumar, S.; Lee, J. C. *Prog. Med. Chem.* **2001**, *38*, 1; (b) Lee, J. C.; Laydon, J. T.; McDonnell, P. C.; Gallagher, T. F.; Kumar, S.; Green, D.; McNulty, D.; Blumenthal, M. J.; Heyes, J. R. *Nature* **1994**, *372*, 739.
2. For reviews of this area see: (a) Hynes, J., Jr.; Leftheris, K. *Curr. Top. Med. Chem.* **2005**, *5*, 967; (b) Goldstein, D. M.; Gabriel, T. *Curr. Top. Med. Chem.* **2005**, *5*, 1017; (c) Diller, D. J.; Lin, T. H.; Metzger, A. *Curr. Top. Med. Chem.* **2005**, *5*, 953; (d) Dominguez, C.; Powers, D. A.; Tamayo, N. *Curr. Opin. Drug Discovery Dev.* **2005**, *8*, 421.
3. (a) Hynes, J., Jr.; Wu, H.; Pitt, S.; Shen, D. R.; Zhang, R.; Schieven, G. L.; Gillooly, K. M.; Shuster, D. J.; Taylor, T. L.; Yang, X.; McIntyre, K. W.; McKinnon, M.; Zhang, H.; Marathe, P. H.; Doweyko, A. M.; Kish, K.; Kiefer, S. E.; Sack, J. S.; Newitt, J. A.; Barrish, J. C.; Dodd, J.; Schieven, G. L.; Leftheris, K. *Bioorg. Med. Chem. Lett.* **2008**, *18*, 1762; (b) Wrobleski, S. T.; Lin, S.; Hynes, J., Jr.; Wu, H.; Pitt, S.; Shen, D. R.; Zhang, R.; Gillooly, K. M.; Shuster, D. J.; Taylor, T. L.; McIntyre, K. W.; Doweyko, A. M.; Kish, K.; Kiefer, S. E.; Tredup, J. A.; Duke, G. J.; Sack, J. S.; McKinnon, M.; Dodd, J.; Barrish, J. C.; Schieven, G. L.; Leftheris, K. *Bioorg. Med. Chem. Lett.* **2008**, *18*, 2739.
4. (a) Burling, F. T.; Goldstein, B. M. *Acta Crystallogr., Sect. B* **1993**, *49*, 738; (b) Haginoya, N.; Kobayashi, S.; Komoriya, S.; Yoshino, T.; Suzuki, M.; Shimada, T.; Watanabe, K.; Hirokawa, Y.; Furugori, T.; Nagahara, T. *Journal Med. Chem* **2004**, *47*, 5167; (c) Hayashi, K.; Ogawa, S.; Sano, S.; Shiro, M.; Yamaguchi, K.; Sei, Y.; Nagao, Y. *Chem. Pharm. Bull.* **2008**, *56*, 802.
5. *General procedure for borylation:* To a solution of *tert*-butyl 5-bromothiazol-2-yl(isopropyl)carbamate (1.87 g, 5.79 mmol) in THF at −78 °C was added *n*-BuLi (2.5 M in hexane, 6.37 mL, 6.36 mmol) dropwise. After stirring at −78 °C for 30 min, 2-isopropoxy-4,4,5,5-tetramethyl-1,3,2-dioxaborolane was added and stirred at −78 °C for 1 h and rt for 2 h. The reaction mixture was quenched with addition of satd aq NH$_4$Cl. The THF was removed under vacuum and the aqueous portion was extracted with EtOAc (40 mL × 3). The combined organics were washed with brine, dried over Na$_2$SO$_4$, filtered and concentrated to afford 2.06 g (96%) as a light yellow solid. ^{1}H NMR (400 MHz, CDCl$_3$) δ ppm 7.86 (1H, s), 5.23 −5.49 (1H, m), 1.59 (9H, s), 1.44 (6H, d, *J* = 6.61 Hz), 1.32 (12H, s).
6. *Experimental procedure for p38α assay:* The assays were performed in V-bottomed 96-well plates. The final assay volume was 60 µL prepared from three 20 µL additions of enzyme, substrates (MBP and ATP) and test compounds in assay buffer (50 mM Tris pH 7.5, 10 mM MgCl$_2$, 50 mM NaCl and 1 mM DTT). Bacterially expressed, activated p38α was pre-incubated with test compounds for 10 min prior to initiation of reaction with substrates. The reaction was incubated at 25 °C for 45 min and terminated by adding 5 µL of 0.5 M EDTA to each sample. The reaction mixture was aspirated onto a pre-wet filtermat using a Skatron Micro96 Cell Harvester (Skatron, Inc.), then washed with PBS. The filtermat was then dried in a microwave oven for 1 min, treated with MeltilLex A scintillation wax (Wallac), and counted on a Microbeta scintillation counter Model 1450 (Wallac). Inhibition data were analyzed by nonlinear least-squares regression using Prism (GraphPadSoftware). The final concentration of reagents in the assays are ATP, 1 µM; [γ-^{33}P]ATP, 3 nM; MBP (Sigma, #M1891), 2 µg/well; p38, 10 nM; and DMSO, 0.3%.
7. *Experimental procedure for PBMC assay:* Heparinized human whole blood was obtained from healthy volunteers. Peripheral blood mononuclear cells (PBMCs) were purified from human whole blood by Ficoll-Hypaque density gradient centrifugation and resuspended at a concentration of 5×10^6/mL in assay medium (RPMI medium containing 10% fetal bovine serum). Fifty microliters of cell suspension was incubated with 50 µL of test compound (4× concentration in assay medium containing 0.2% DMSO) in 96-well tissue culture plates for 5 min at rt. Hundred microliters of LPS (200 ng/mL stock) was then added to the cell suspension and the plate was incubated for 6 h at 37 °C. Following incubation, the culture medium was collected and stored at −20 °C. TNF-α concentration in the medium was quantified using a standard ELISA kit (Pharmingen-San Diego, CA). Concentrations of TNF-α and IC$_{50}$ values for test compounds (concentration of compound that inhibited LPS-stimulated TNF-α production by 50%) were calculated by linear regression analysis.
8. Kinase selectivity data determined for **41** based on Ambit screening at 10 µM: no activity observed (100% of control) for the following kinases: ABL1, AMPKA1, AURA, AURC, CAMK1A, CAMK1D, CDK2, CK1E, CLK1, CSK, DAPK2, EGFR, EPHA2, EPHB4, FGF1R, FLT3, GAK, IGF1R, INSR, KDR, MAP3K4, MARK2, MNK2, NEK2, PAK1, PAK4, PAK5, PHKG1, PIM1, SKMLCK, SRC, STK16, SYK, TIE2, TRKA. Activity observed as% of control: JNK1 (24.9%), JNK3 (0.2%), KIT (14.5%), PDGRB (11.3%), p38α (0%).